Physica E 124 (2020) 114223

Contents lists available at ScienceDirect

Physica E: Low-dimensional Systems and Nanostructures

journal homepage: http://www.elsevier.com/locate/physe

Ligand engineering of mid-infrared Ag_2Se colloidal quantum dots

Shihab Bin Hafiz [a], Mohammad M. Al Mahfuz [a], Michael R. Scimeca [b], Sunghwan Lee [c], Soong Ju Oh [d], Ayaskanta Sahu [b], Dong-Kyun Ko [a,*]

[a] Department of Electrical and Computer Engineering, New Jersey Institute of Technology, Newark, NJ, 07102, United States
[b] Department of Chemical and Biomolecular Engineering, New York University, Brooklyn, NY, 11201, United States
[c] School of Engineering Technology, Purdue University, West Lafayette, IN, 47907, USA
[d] Department of Materials Science and Engineering, Korea University, 02841, Republic of Korea

ARTICLE INFO

Keywords:
Colloidal quantum dots
Surface ligands
Mid-infrared
Photodetectors
Responsivity

ABSTRACT

Silver selenide colloidal quantum dots exhibit distinct optical absorption in the mid-wavelength infrared spectral region, which arises from the intraband transition between the first and the second quantum-confined energy levels. The optical absorption coefficient, carrier mobility, and carrier lifetime, which are the three primary parameters that determine the ultimate performance of a photodetector, are expected to be heavily dependent on the surface capping ligands. Herein, we characterize these parameters on silver selenide colloidal quantum dots films chemically treated with ligands selected from literatures that report high-performance quantum dot-based solar cells, photodetectors, transistors, and thermoelectrics. We correlate these results with the mid-infrared responsivities measured from photoconductive photodetectors fabricated from respective ligand-exchanged films. The insights gained from this study may serve as a foundation for enabling future intraband CQD-based MWIR sensing and imaging technologies.

1. Introduction

Photodetectors operating in the atmospheric transmission window of mid-wavelength infrared (MWIR = 3–5 μm) are finding growing number of applications that require low size, weight, power consumption and cost (SWAP-C) [1]. A significant reduction in SWAP-C is possible with the development of MWIR photodetectors that can achieve high sensitivity without cryogenic cooling [2,3]. Colloidal quantum dot (CQD) photodetectors are a promising technology that have the potential to enable high temperature operation. In particular, intraband CQDs — an emerging subset of CQD technology that utilize optical transitions between the first and the second quantum confined energy levels — have been studied to show strong suppression of Auger relaxation [4], a carrier recombination process that has been the primary culprit for reduced photodetector sensitivity at elevated temperature in bulk semiconductor devices [5,6]. This suppression mechanism is found to originate from the sparse density of states of CQDs, a generic feature found in quantum-confined nanoparticle systems. Mercury selenide (HgSe) represents the current leading intraband MWIR CQD technology that has been reported to show uncooled detectivity of 10^8 Jones, a performance comparable to commercial deuterated triglycine sulfate (DTGS) detectors [7]. Silver selenide (Ag_2Se) is a MWIR CQD that has recently expanded the family of intraband CQDs [8] and it is uniquely free of heavy metals. Our group [9,10] and others [11] have recently investigated the device characteristics of photoconductive photodetector fabricated from Ag_2Se CQDs, demonstrating appreciable room temperature responsivity (0.21 mA/W at 4.5 μm radiation under applied bias of 0.2 V, 60–80 nm CQD film thickness, 1,2-ethanedithiol ligands).

Irrespective of device types and structures (e.g. photoconductor, Schottky diode, or p-n junction diode), photodetection is governed by two fundamental steps of device operation: (1) optical absorption and (2) carrier separation and extraction [1]. The absorption coefficient of CQD film determines the magnitude of process (1) and the carrier mobility-lifetime product dictates the efficiency of process (2). It is well known that ligand exchange, a process where original long and bulky capping ligands are exchanged with a shorter one to create electrically conductive CQD films [12,13], heavily influences these three key material parameters [14,15] (absorption coefficient, carrier mobility, and carrier lifetime). However, there are no systematic ligand studies on the Ag_2Se CQD system reported to date. Herein, we characterize these parameters on films chemically treated with ligands selected from literatures that report the high-performance solar cells, photodetectors,

* Corresponding author.
E-mail address: dkko@njit.edu (D.-K. Ko).

https://doi.org/10.1016/j.physe.2020.114223
Received 9 March 2020; Received in revised form 2 May 2020; Accepted 18 May 2020
Available online 22 May 2020

transistors, and thermoelectrics. Based on these results, we fabricate photoconductive photodetectors from top candidate ligand-exchanged films and correlate the magnitude of mid-infrared responsivities to gain an insight into the material property-device performance relationship.

2. Chemicals and experimental methods

Oleylamine (70%), trioctylphosphine (90%), selenium (100 mesh, 99.5+ %), silver chloride (99%), 1-butanol (anhydrous, 99.8%), ethyl alcohol (200 proof, > 99.5%), methanol (anhydrous, 99.8%, Sigma), hexane (ACS reagent grade), octane (anhydrous, 99%), arsenic sulfide (>99.99%), propylamine (99+ %), 1,2-ethanedithiol (EDT, > 98%), ammonium thiocyanate (NH_4SCN, 97.5+ %), tetrabutylammonium iodide (TBAI, > 99%), and ethylenediamine (EDA, > 99%)) were purchased from Sigma-Aldrich and were used as received.

2.1. Synthesis of Ag_2Se CQDs

Ag_2Se CQDs having MWIR absorption peak centered at 5 μm were synthesized by modifying the previously reported procedure [16]. Briefly, 15 mL of oleylamine was added to a three-neck flask under vacuum and the temperature was raised to 90 °C for 1 h. 1 M TOP-Se and 0.5 M TOP-Ag, were prepared though dissolving Se powder and AgCl in TOP, respectively, inside the glovebox. 2 mL of 1.0 M TOP-Se was added to oleylamine after switching the atmosphere to nitrogen environment and the temperature of the mixture was increased to 170 °C. Then, 2 mL of 0.5 M TOP-Ag was quickly injected to initiate the Ag_2Se CQD formation. The color of the mixture turned to dark brown immediately. The reaction was terminated after 5 s by injecting 10 mL of butanol and cooling using a water bath. The CQDs were then precipitated with a mixture of ethanol and methanol. After centrifugation, the final precipitate was redispersed in a mixture of hexane and octane after two methanol washes (see Supplementary material).

2.2. Fabrication of CQD film

Ag_2Se CQD films were fabricated on ZnSe (for optical measurements) discs or on Si/SiO_2 substrates (for device measurements). Drop casting was used to deposit a film and subsequent ligand exchange was performed. For As_2S_3, 0.8 M ligand exchange solution was prepared by dissolving As_2S_3 powder in polypropylamine. The solution was then diluted in ethanol and ligand exchange has been performed by dipping CQD films in the diluted solution and washed with pure ethanol, following the previously reported protocol [17]. For 1,2-ethanedithiol (EDT), ammonium thiocyanate (NH_4SCN), tetrabutylammonium iodide (TBAI), and ethylenediamine (EDA) ligand exchange, solution containing 0.1 M EDT, 0.15 M NH_4SCN, 0.02 M TBAI, and 0.1 M EDA, all in methanol, were prepared for dipping and the sample film was washed with pure methanol after the exchange process. A layer-by-layer film deposition and ligand exchange was repeatedly performed to create a thick CQD film.

2.3. Optical characterization

The sample films deposited on ZnSe discs were prepared following the procedure described above. The absorption spectra were obtained using a Thermo Nicolet 370 FTIR spectrometer in transmission configuration. The CQD film thickness was measured using atomic force microscopy (Bruker Dimension Icon AFM).

2.4. Electrical characterization

The carrier concentration and mobility of the ligand exchanged CQD films were measured by Hall effect measurement system, using a 0.5 T fixed magnet in a 4-probe chamber (H-5000, MMR Technologies). A standard van der paw configuration was used.

2.5. Optoelectronic characterization

A calibrated blackbody (Newport 67,030, 900 °C) filtered with Ge was used as an excitation source and an Agilent 4155 semiconductor parameter analyzer was used to measure the current as a function of time.

2.6. Device fabrication and testing

Photoconductive photodetector devices were fabricated by depositing CQD film formed via layer-by-layer CQD deposition and ligand exchange, onto Si/SiO_2 substrates with pre-patterned interdigitated electrodes (Cr/Au). The channel length and width were 10 μm and 64.9 mm, respectively. A calibrated blackbody (Newport 67,030, 900 °C) coupled with 5 μm bandpass filter was used as an illumination source. The photocurrent was measured using SR570 preamplifier and SR930 lock in amplifier. A Joule-Thomson cooling chamber (MMR Technologies) was used to cool the device down to 90 K.

3. Results and discussion

3.1. Characterization approaches

We start with a brief discussion on our characterization approaches. First, we characterize the optical absorption coefficient of ligand-exchanged Ag_2Se CQD film following the previously reported procedure on HgTe CQD film [18]. The absorption coefficient (α) is calculated from the percent transmission ($\%T$) of the film measured using Fourier transform infrared spectroscopy (FTIR) and film thickness (t) estimated using atomic force microscopy (AFM) as:

$$\alpha = \frac{2.303 * log_{10}\left(\frac{100}{\%T}\right)}{t}$$

The $\%T$ obtained from each CQD film is shown in Fig. 1 and Table 1 summarizes the results of α.

Field-effect transistor (FET) characteristic measurement has been used as a common way to characterize the carrier mobility of a CQD film [19,20]. However, due to the heavily-doped nature of the Ag_2Se CQD film, FETs show negligible gate response, making mobility value extraction challenging, as we have reported in our previous study [10]. We estimate the carrier mobility (and concentration) of our CQD film using Hall effect measurements. Performing Hall effect measurement on systems exhibiting hopping conduction is known to yield anomalous Hall signs [21,22]. Especially for film having low carrier mobility ($\ll 1$ $cm^2V^{-1}s^{-1}$), reliable measurement becomes difficult since induced Hall voltage typically becomes much lower than the large offset background voltage [23]. Such was observed in our EDT treated CQD film yielding random positive and negative Hall signs. On the other hand, strongly coupled CQD film that shows band-like conduction have been reported with reliable mobility values, in close agreement with mobility values extract from FET analysis [24–26]. Indeed, in our Ag_2Se CQD films treated with As_2S_3 and NH_4SCN, high and reliable mobility values were measured with consistent negative Hall signs (majority carrier electrons). Table 2 summarizes the Hall effect measurement results obtained from each ligand-exchanged CQD film. Anomalously high mobilities observed in TBAI and EDA sample films are possibly due to CQD fusion, which are discussed later in detail.

As for the carrier lifetime measurements, the lifetime of photogenerated carriers in CQDs are typically obtained from time-resolved photoluminescence (PL) measurements. However, this becomes challenging for CQDs having very narrow energy gap with intrinsically low luminescence efficiencies, especially for CQD films that are ligand-exchanged [27]. Also, this PL lifetime does not represent the carrier behavior in CQD film under biased operation (when carriers are under

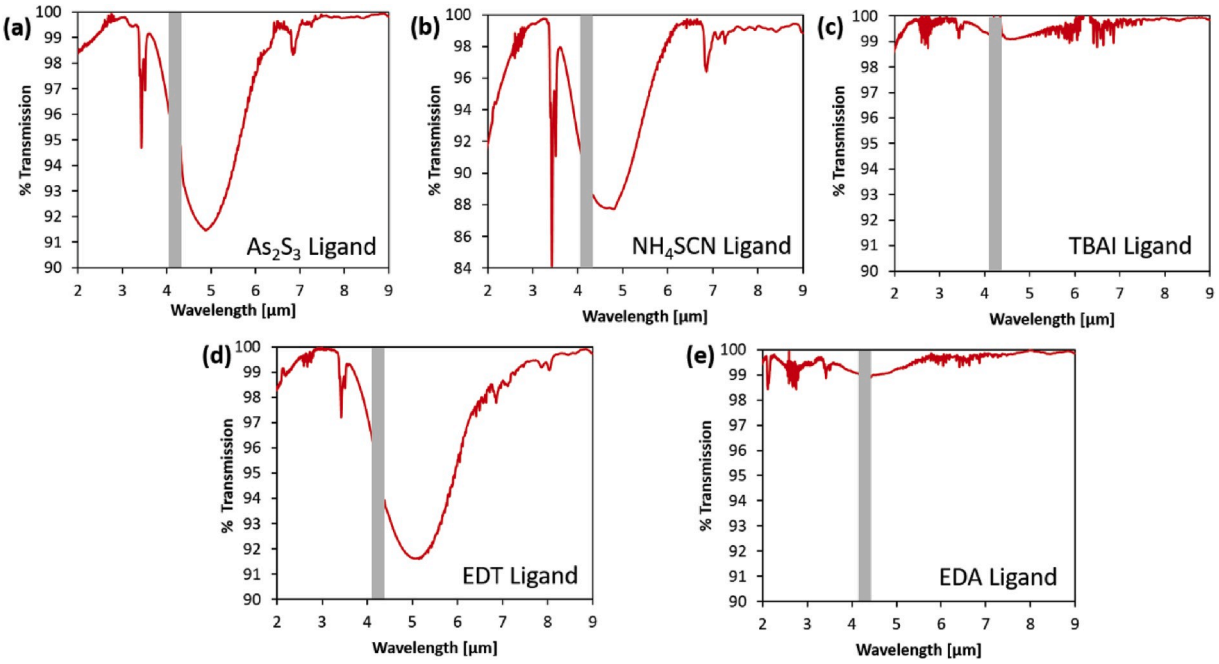

Fig. 1. Percent transmission obtained using FTIR measurement on Ag_2Se CQD films treated with (a) As_2S_3-based metal-chalcogenide complex, (b) NH_4SCN thiocyanate, (c) atomic halide TBAI, (d) stand organic EDT, and (e) organic EDA ligands. Peaks around 4.25 μm (2350 cm^{-1}) that arise from background CO_2 are omitted for clarity.

Table 1
Table summarizing the absorption coefficient measurement results of Ag_2Se QD film treated with 5 candidate ligands.

Ligand Types	% of Transmission at 5 μm peak **[%]**	Film thickness [cm]	Absorption Coefficient [cm^{-1}]
Metal-Chalcogenide Complex (As_2S_3)	91.5	(460 ± 30) x10^{-7}	(1.9 ± 0.1) x10^3
Thiocyanate Ligand (NH_4SCN)	84.1	(180 ± 20) x10^{-7}	(4.5 ± 0.3) x10^3
Halide Ligand (TBAI)	99.1	(420 ± 10) x10^{-7}	230 ± 10
1,2-Ethanedithiol (EDT)	91.6	(88 ± 5) x10^{-7}	(9.5 ± 0.5) x10^3
Ethylenediamine (EDA)	99	(230 ± 20) x10^{-7}	440 ± 40

transport). Carrier lifetimes extracted from transient photocurrent measurement yield more relevant information about the CQD films used in devices and hence was the method performed in this study. All ligand-exchanged Ag_2Se CQD films were characterized by a long decay transient, i.e. photocurrent decay occurring <100 ms constitute less than 6% of overall photocurrent decay whereas, majority of 94% photocurrent decay occurs at a timescale of tens of seconds (Fig. 2). Thus, we extract the carrier lifetime using long time traces. Sample CQD films were cooled to 90 K and a calibrated blackbody with Ge filter, which cuts off photons with wavelength shorter than 2 μm (thus, only using mid-wavelength and long-wavelength IR photons), was used as a photoexcitation source. Photocurrent transient decay and data fitting to calculate carrier lifetime are shown in Fig. 2. For TBAI- and EDA-treated CQD films, due to the significant reduction in MWIR absorbance after ligand exchange, photocurrent transients could not be obtained.

3.2. *Property characterization of Ag_2Se CQD films ligand-exchanged with various ligands*

Based on these characterization approaches, the following describes the analysis results on Ag_2Se CQD films treated with 5 selected ligands,

Table 2
Table summarizing the Hall effect measurement results of Ag_2Se QD film treated with 5 candidate ligands. * Denotes anomalous Hall mobility value arising from possible QD fusion. † Denotes Hall effect measurement that did not yield reliable results due to the low carrier mobility as Hall voltage becomes extremely low. This typically occurs when carrier mobility in the film is well below 1 $cm^2V^{-1}s^{-1}$ whereby extracting Hall voltage from large offset background becomes difficult [19]. The majority carrier type of electron for EDT ligand-exchanged film has been determined using Seebeck measurement in our previous report [10].

Ligand Types	Sheet Resistance [Ω/sq]	Carrier Density [cm^{-3}]	Mobility [$cm^2V^{-1}s^{-1}$]	Majority Carrier
Metal-Chalcogenide Complex (As_2S_3)	1.08×10^6	1.68×10^{16}	11.3	Electrons
Thiocyanate Ligand (NH_4SCN)	1.11×10^4	8.85×10^{17}	19.4	Electrons
Halide Ligand (TBAI)	1.52×10^2	3.75×10^{18}	439*	Electrons
1,2-Ethanedithiol (EDT)	3.87×10^5	Not measurable†	$\ll 1$†	Electrons
Ethylenediamine (EDA)	1.26×10^3	1.93×10^{17}	1030*	Electrons

along with a rationale behind the choice of each ligand.

3.2.1. *Metal-chalcogenide complexes based on As_2S_3*

Our first ligand choice is the molecular metal chalcogenide complex $(NH_4)_3AsS_3$ which replaces the parent oleylamine ligand attached on the CQD surface to inorganic As_2S_3 capping shell. The metal chalcogenide ligands have been widely reported to yield high field-effect mobilities due to the reduction in transport energy barriers compared to the standard organic ligands [28]. Notably, mobility values exceeding 400 $cm^2V^{-1}s^{-1}$ have been demonstrated for CdSe CQD films with composition-matched Cd_2Se_3-based capping ligands [29]. As_2S_3-based capping ligand used in this study, in particular, is transparent in the mid-infrared [7] whereas typical organic ligands have characteristic mid-infrared absorption signatures, which adds to a significant

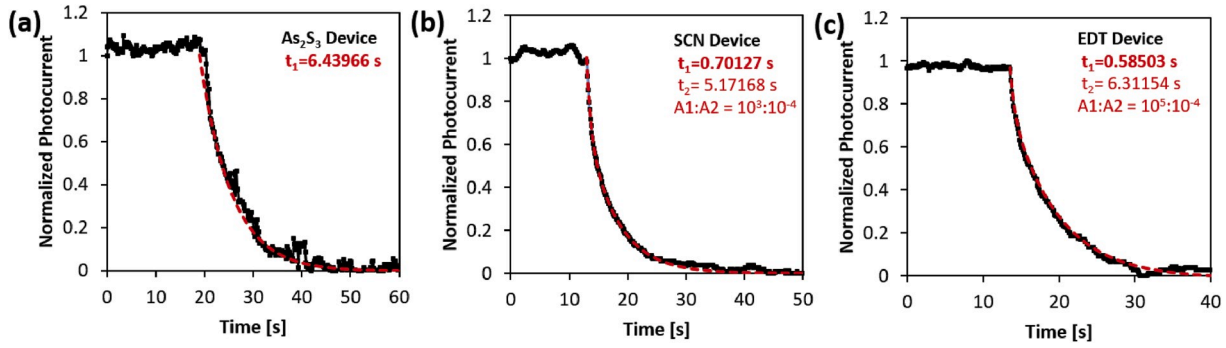

Fig. 2. Transient photocurrent decay data obtained from photoconductive devices fabricated from (a) As_2S_3, (b) NH_4SCN, and (c) EDT treated CQD film at 90 K. The data in (a) can be fitted to a single exponential function with characteristic lifetime of t_1 while (b) and (c) are fitted to a biexponential equation having t_1 and t_2 lifetimes with pre-exponential factors of *A1* and *A2*, respectively.

motivation for our study. Indeed, in our Ag_2Se QD films, high electron mobility of ≈10 $cm^2V^{-1}s^{-1}$ is observed. In fact, this is consistent with the previous report on HgSe QDs where ligand exchange to As_2S_3 yields electron mobility of 90 $cm^2V^{-1}s^{-1}$ with highest detectivity of 10^8 Jones reported to date for intraband CQD-based devices [7]. The optical absorption coefficient (≈10^3 cm^{-1}) is also comparable to HgTe QDs (3×10^3 cm^{-1}) [18] which is currently the leading mid-infrared CQD (interband) material.

The photocurrent decay obtained from Ag_2Se CQD films treated with As_2S_3 complex ligands can be fitted to a single exponent with a carrier lifetime of $\tau_1 = 6.4$ s, the longest lifetime of all films investigated. Such long characteristic time constants, up to tens of seconds, have been widely observed in CQD-derived films [30,31] and has been assigned to originate from deep trap states. Combined with the mobility value, As_2S_3 ligand exchanged films show the highest carrier mobility-lifetime product of 72.3 cm^2/V.

3.2.2. Thiocyanate ligand: NH_4SCN

Our second ligand is the thiocyanate (NH_4SCN) ligand, which has also been studied to exhibit high field-effect mobility of 27 $cm^2V^{-1}s^{-1}$ [26], a high value reminiscent of a band-like transport. Applying this ligand to our Ag_2Se CQD films results in both high electron mobility (19.4 $cm^2V^{-1}s^{-1}$) and high absorption coefficient (≈10^3 cm^{-3}), making it one of the top candidates to pursue further as photodetector devices.

A bi-exponential equation with characteristic carrier lifetime of $\tau_1 = 0.7$ s and $\tau_2 = 5.2$ s gives an accurate fitting to the photocurrent decay (Fig. 2b), indicating an energetic distribution of trap states [30]. However, the pre-exponential factor (weight) of long τ_2 lifetime component is negligibly small (10^{-7} times smaller than τ_1 component) than τ_1. Based on predominant τ_1 lifetime value, CQD films treated with NH_4SCN show the highest mobility among the list of ligands (excluding anomalous values) resulting in a carrier lifetime product of 13.6 cm^2/V.

3.2.3. Atomic halide ligand: TBAI

Atomic halide ligands (tetrabutylammonium iodide, TBAI), which is the third choice of our study, have been frequently employed in fabricating CQD solar cells to yield high photovoltaic efficiencies [32,33]. The high efficiencies have been studied to arise from improved surface passivation compared to the organic ligand counterparts, owing to their small sizes (I^- ion) and hence reduced steric hindrance. Employing this ligand to Ag_2Se CQDs, however, unexpectedly led to a large reduction in MWIR absorbance (Fig. 1c). Reductions in optical absorbance after ligand exchange have been previously observed in HgSe CQD films, originating from dedoping effect [14]. Reducing the number of electrons populating the first conduction state $1S_e$ will weaken the $1S_e$ to $1P_e$ (second conduction state) optical transition, thereby reducing the corresponding absorbance. However, this is not in agreement with the electron density measured in our TBAI ligand exchanged CQD films (Table 2), which shows higher electron concentration than As_2S_3 and NH_4SCN treated films. An alternative explanation is the occurrence of CQD fusion after TBAI ligand exchange. In fact, the observation of atomic ligand exchange-induced CQD fusion is not new and has been previously reported as a novel method of creating epitaxially-connected CQD superlattice films [34,35]. A significant fusion in Ag_2Se CQD film may lead to a near-complete relaxation of quantum confinement, which will wash away the distinct absorption feature in the mid-infrared. In addition, phase change from tetragonal to orthorhombic is possible, if the fusion results in a grain size larger than 38 nm [36]. The occurrence of CQD fusion is also supported by anomalously high carrier mobility of 439 $cm^2V^{-1}s^{-1}$ that resembles the magnitude observed in bulk Ag_2Se thin-films. Polycrystalline Ag_2Se thin-films have been reported to have high electron mobility, reaching 1000 $cm^2V^{-1}s^{-1}$ even at carrier concentration in the excess of 10^{18} cm^{-3} [37,38]. Overall, both optical and electronic property characterization results points to an occurrence of CQD fusion. More chemical, structural, and morphological studies are currently on the way to elucidate the detailed mechanism. On the other hand, due to an orders of magnitude reduction in MWIR absorption, photocurrent decay measurement was not possible. It is concluded that while these films yield very high carrier mobilities, small absorbance in the MWIR spectral region renders them ineffective for use in photodetection.

3.2.4. Standard organic ligand: EDT

The fourth ligand is 1,2-ethanedithiol (EDT) which has been used widely in the CQD device community as a standard, compact organic ligand [39,40]. While this ligand yields the highest absorption coefficient (≈9×10^3 cm^{-1}), the carrier mobility is below our measurement limit of DC Hall effect [23]. This indicates that the mobility is significantly below ≪ 1 $cm^2V^{-1}s^{-1}$. The closest system is the intraband HgSe CQD film which has a reported mobility of 6×10^{-4} $cm^2V^{-1}s^{-1}$ with identical EDT treatment [41]. The photocurrent transient decay data obtained from EDT-treated Ag_2Se CQD film shows a carrier lifetime of $\tau = 0.58$ s, a similar timescale to NH_4SCN treated films.

3.2.5. Organic ligand with different functional group: EDA

The final ligand is ethylenediamine (EDA). In comparison to the standard EDT ligand that demonstrates the amine-to-thiol ligand exchange, EDA enables us to investigate amine-to-amine ligand exchange. The significant reduction in absorption coefficient and anomalously high value of electron mobility (1030 $cm^2V^{-1}s^{-1}$) suggest that CQD fusion and film microstructural changes may be taking place in EDA-treated CQD film, similar to that of TBAI ligands. Due to absence in MWIR absorption, photocurrent decay measurement was not possible. The negligible absorption in the mid-infrared makes this ligand ineffective for photodetector applications.

3.3. Measurement of device characteristics of Ag_2Se CQD-based photodetectors

Based on above property characterizations, photoconductive photodetector devices of As_2S_3, NH_4SCN, and EDT ligand-exchange CQD films were fabricated for MWIR responsivity characterization. The measurement was performed by illuminating the CQD film at 5 μm (resonating with the CQD absorption peak) and measuring the photocurrent using lock-in technique. A schematic of our responsivity measurement setup is shown in Fig. 3a. The spectral irradiance of our 900 °C calibrated black body was calculated using Plank radiation formula and the irradiance filtered through 5 μm bandpass filter is plotted using the transmission data provided by the manufacturer, as shown in Fig. 3b. The area under the blue curve corresponds to radiant emittance of $W_R = 0.46$ W/cm^2. The optical power of incident 5 μm radiation was estimated using $P = A \cdot W_R \cdot \frac{a^2}{4d^2} \cdot t \cdot \eta$ where, $A = 6.49 \times 10^{-3}$ cm^2 is the active sensor area, $a = 2.54$ cm is the diameter of source aperture, $d = 13.5$ cm is the source aperture to device distance, $t = 0.92$ is the transmission of optical pass, and $\eta = 1.33$ is the amplification factor due to concentration of parabolic mirror. The optical power is $P = 32.32$ μW in our setup. The responsivity value is calculated by dividing the measured photocurrent with this optical power. Fig. 4 shows the device responsivity measurement results obtained at 90 K.

3.3.1. Devices based on As_2S_3 treated CQD film

The device made from Ag_2Se CQD films treated with As_2S_3-based ligands, which is expected to show the best device performance, exhibit the lowest responsivity of 0.41 mA/W of the three candidate devices. As the carrier mobility-lifetime product is the highest, this device is expected to have the highest carrier collection efficiency. The observed low photocurrent indicate that a different recombination mechanism is present, other than non-germinate recombination that photocarriers experience during transport. Other recombination mechanisms frequently discussed in CQD system are the monomolecular (germinate) recombination where photogenerated exciton recombine at the single CQD level before splitting into separate electron and hole photocarriers. This can occur if the ligand exchange creates large density of defects at the CQD surface. The low absorption coefficient ($\alpha = 1.9 \times 10^3$ cm^{-1}) combined with high rate of monomolecular recombination due to defective surface may thus lead to the lowest amount of photocarriers initially. The reason behind why As_2S_3 specifically induces monomolecular recombination active surface defects is unclear and require further study.

In photoconductive devices, the driving force for exciton separation is provided by the external applied bias. Increasing the bias would enable charge separation to occur more effectively thereby minimizing the monomolecular recombination. However, we have found that Ag_2Se CQD devices can operate only at small bias ranges, typically <4 V (4000 V/cm), and increasing the bias irreversibly damages the CQD film due to high diffusive nature of Ag + ions that compose the CQDs. This seems to be the limitation of current generation Ag_2Se CQD devices. For a comparison, PbS CQD have shown to operate up to 100 V bias (2×10^5 V/cm, while not practical) to demonstrate high responsivity [42]. If high biasing was possible in Ag_2Se CQD, it is anticipated that a regime change from germinate to non-germinate recombination will occur and thus, As_2S_3 treated device would exhibit the top responsivity. Hybrid ligand strategy have been previously demonstrated in CQD solar cell research with great success [43]. Following the first ligand exchange, which effectively reduces the inter-CQD spacing to enhance the carrier mobility, a second ligand exchange is performed (second ligand is usually smaller than the first ligand) with a purpose of improving the surface passivation. This strategy could be adopted, if appropriate atomic-sized ligand can be identified that can remedy the surface defects while preserving the MWIR absorbance.

Reflecting the fact that these CQD films show long characteristic carrier lifetimes, a photoconductive gain mechanism may be present that may lead to a greatly amplified responsivity [31]. In our As_2S_3 treated CQD devices, the transit time ($\tau_{tr} = L^2/\mu V_{SD}$) of 4.42×10^{-8} s can be estimated from the carrier mobility ($\mu = 11.3$ cm^{2}V^{-1}s^{-1}), channel length ($L = 10$ μm), and source-drain bias ($V_{SD} = 2$ V). Taking the carrier lifetime of 6.4 s, a high gain on the order of 10^8 can be theoretically reached. However, this would not be measured through the lock-in detection technique employed here. The optical chopping frequency of 15 Hz indicate that the illumination repeats on/off cycle every 0.06 s, much before the photocurrent rises to a higher saturation value which is expected to take at least several seconds (Fig. 2). While the photoconductive gain would lead to a greater photodetector sensitivity, the slow time response typically makes them impractical for many fast sensing or imaging applications.

3.3.2. Devices based on NH_4SCN treated CQD film

The devices fabricated from CQD treated with NH_4SCN have lower carrier-lifetime product but higher absorption coefficient than As_2S_3-treated CQD devices. The measured MWIR responsivity is also higher

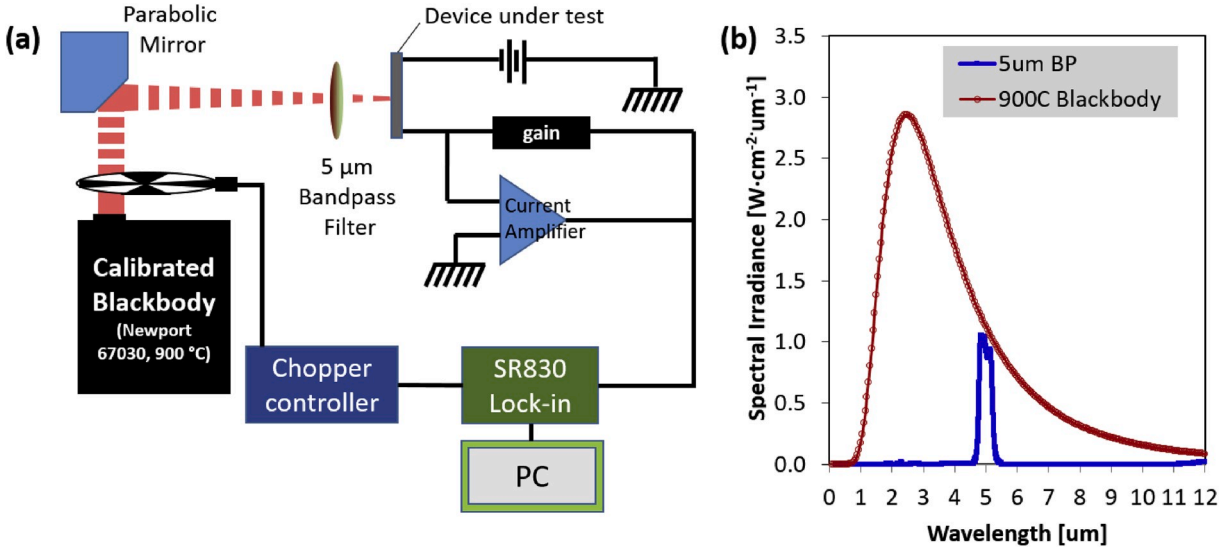

Fig. 3. A schematic of (a) responsivity measurement setup. (b) Shows spectral irradiance plots of 900 °C blackbody and the blackbody irradiance filtered through 5 μm bandpass filter.

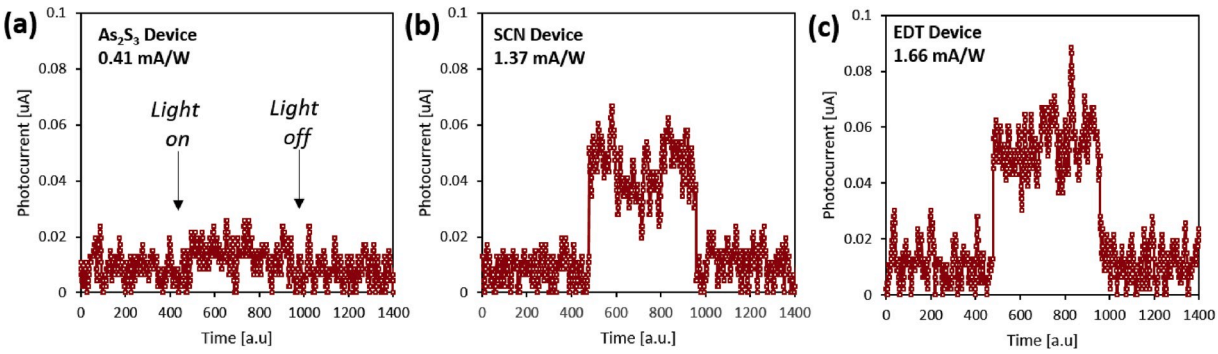

Fig. 4. Photocurrent measurement data of (a) As_2S_3, (b) NH_4SCN, and (c) EDT treated CQD devices obtained using 5 μm MWIR illumination at 90 K.

(1.37 mA/W). If monomolecular recombination is the dominant mechanism in these devices as well, it is expected that higher absorption coefficient is primarily responsible for the observed higher responsivity.

3.3.3. Devices based on standard organic EDT treated CQD film

With similar carrier lifetime to SCN devices, organic EDT treated CQD device exhibit the highest responsivity of 1.66 mA/W. This is surprising, reflecting the fact that the mobility is expected to be $\ll 1$ $cm^2V^{-1}s^{-1}$. This suggests that while carrier collection is not as efficient, the photocarrier separation and thus the extent of surface passivation is greater than SCN and As_2S_3 treated CQD devices. The largest absorption coefficient (9.5×10^3 cm^{-1}) combined with better surface passivation could be accounted for the high responsivity observed in this study. This again suggests that the separation of photocarriers, rather than carrier collection efficiency, is the limiting factor of our Ag_2Se CQD devices.

Table 3 summarizes the infrared responsivity at 5 μm. The magnitude of the device responsivity is the order of EDT > NH_4SCN > As_2S_3. Our finding is in stark contrast to commonly studied MWIR HgTe and HgSe CQD devices, where top device performance is obtained from As_2S_3 treated devices due to high carrier mobility-lifetime product (maximum carrier collection efficiency) [7,27]. The correlation between the material property characterizations and device performance results suggests that having maximum optical absorption and minimum monomolecular recombination (thus, maximum generation of photocarriers) is an important factor that determines the ultimate responsivity of our current generation of Ag_2Se CQD device.

4. Conclusion

In summary, we have investigated five candidate ligands for intraband Ag_2Se CQDs film and characterized three key properties that determine the performance of photodetector devices. These results were correlated with MWIR responsivities obtained for device fabricated from respective ligand-exchanged CQD films. Based on the analysis between the material property and device performance, we discuss that having maximum optical absorption and minimum monomolecular recombination (thus, maximum generation of photocarriers) is an important factor that determines the ultimate responsivity of our current generation of devices. Due to limited bias operation range of Ag_2Se CQD-based devices, the future effort should focus on improving the surface passivation. Hybrid ligand approach may point the way to this improvement.

Declaration of competing interest

The authors declare that they have no known competing financial interests or personal relationships that could have appeared to influence the work reported in this paper.

Table 3
Summary of absorption coefficients, mobility-lifetime products, and infrared responsivities of ligand exchanged Ag_2Se CQD films.

Ligand Types	Absorption Coefficient [cm^{-1}]	Mobility-Lifetime Product [cm^2/V]	Responsivity at 5 μm [mA/W]
Metal-Chalcogenide Complex (As_2S_3)	$(1.9 \pm 0.1) \times 10^3$	72.3	**0.41**
Thiocyanate Ligand (NH_4SCN)	$(4.5 \pm 0.3) \times 10^3$	13.6	**1.37**
1,2-Ethanedithiol (EDT)	$(9.5 \pm 0.5) \times 10^3$	N/A	**1.66**

CRediT authorship contribution statement

Shihab Bin Hafiz: Investigation, Validation, Writing - original draft. **Mohammad M. Al Mahfuz:** Investigation, Validation. **Michael R. Scimeca:** Investigation, Validation. **Sunghwan Lee:** Methodology, Validation, Writing - review & editing. **Soong Ju Oh:** Methodology, Validation, Writing - review & editing. **Ayaskanta Sahu:** Conceptualization, Funding acquisition, Writing - review & editing. **Dong-Kyun Ko:** Supervision, Conceptualization, Funding acquisition, Writing - review & editing.

Acknowledgements

This work is/was supported by Global Research Outreach program of Samsung Advanced Institute of Technology as well as US National Science Foundation Grant No. ECCS-1809112 (DK) and ECCS-1809064 (AS). We also gratefully acknowledge support for instrument use, scientific and technical assistance from the NYU Shared Instrumentation Facility through the Materials Research Science and Engineering Center (MRSEC) and MRI programs of the National Science Foundation under Award numbers DMR-1420073 and DMR-0923251 and the Imaging and Surface Science Facilities of Advanced Science Research Center at the Graduate Center of CUNY.

Appendix A. Supplementary data

Supplementary data to this article can be found online at https://doi.org/10.1016/j.physe.2020.114223.

References

[1] S.B. Hafiz, M. Scimeca, A. Sahu, D.K. Ko, Colloidal quantum dots for thermal infrared sensing and imaging, Nano Converg 6 (2019) 7.
[2] J. Piotrowski, Uncooled operation of Ir photodetectors, Opto-Electron. Rev. 12 (2004) 111–122.
[3] P. Martyniuk, A. Rogalski, Hot infrared photodetectors, opto-electron, Rev. 21 (2013) 239–257.
[4] C. Melnychuk, P. Guyot-Sionnest, Auger suppression in N-type hgse colloidal quantum dots, ACS Nano 13 (2019) 10512–10519.

[5] A. Rogalski, Hgcdte infrared detector material: history, status and outlook, Rep. Prog. Phys. 68 (2005) 2267–2336.
[6] D. Lee, M. Carmody, E. Piquette, P. Dreiske, A. Chen, A. Yulius, D. Edwall, S. Bhargava, M. Zandian, W. Tennant, High-operating temperature hgcdte: a vision for the near future, J. Electron. Mater. 45 (2016) 4587–4595.
[7] E. Lhuillier, M. Scarafagio, P. Hease, B. Nadal, H. Aubin, X.Z. Xu, N. Lequeux, G. Patriarche, S. Ithurria, B. Dubertret, Infrared photodetection based on colloidal quantum-dot films with high mobility and optical absorption up to thz, Nano Lett. 16 (2016) 1282–1286.
[8] M. Park, D. Choi, Y. Choi, H.-b. Shin, K. Jeong, Mid-infrared intraband transition of metal excess colloidal Ag2se nanocrystals, ACS Photonics 5 (2018) 1907–1911.
[9] S. Hafiz, M. Scimeca, P. Zhao, I. Paredes, A. Sahu, D.-K. Ko, Silver selenide colloidal quantum dots for mid-wavelength infrared photodetection, ACS Appl. Nano Mater. 2 (2019) 1631–1636.
[10] S. Hafiz, M. Scimeca, A. Sahu, D.-K. Ko, Mid-infrared colloidal quantum dot based nanoelectronics and nano-optoelectronics, ECS Trans 92 (2019) 11–16.
[11] J. Qu, N. Goubet, C. Livache, B. Martinez, D. Amelot, C. Greboval, A. Chu, J. Ramade, H. Cruguel, S. Ithurria, M. Silly, E. Lhuillier, Intraband mid-infrared transitions in Ag2se nanocrystals: potential and limitations for Hg-free low-cost photodetection, J. Phys. Chem. C 122 (2018) 18161–18167.
[12] D. Talapin, J.-S. Lee, M. Kovalenko, E. Shevchenko, Prospects of colloidal nanocrystals for electronic and optoelectronic applications, Chem. Rev. 110 (2009) 389–458.
[13] C. Kagan, E. Lifshitz, E. Sargent, D. Talapin, Building devices from colloidal quantum dots, Science 353 (2016) aac5523.
[14] A. Robin, C. Livache, S. Ithurria, E. Lacaze, B. Dubertret, E. Lhuillier, Surface control of doping in self-doped nanocrystals, ACS Appl. Mater. Interfaces 8 (2016) 27122–27128.
[15] K. Jeong, J. Tang, H. Liu, J. Kim, A. Schaefer, K. Kemp, L. Levina, X. Wang, S. Hoogland, R. Debnath, L. Brzozowski, E. Sargent, J. Asbury, Enhanced mobility-lifetime products in pbs colloidal quantum dot photovoltaics, ACS Nano 6 (2011) 89–99.
[16] A. Sahu, A. Khare, D. Deng, D. Norris, Quantum confinement in silver selenide semiconductor nanocrystals, Chem. Commun. 48 (2012) 5458–5460.
[17] E. Lhuillier, S. Keuleyan, P. Zolotavin, G.-S. Philippe, Mid-infrared hgte/As2s3 field effect transistors and photodetectors, Adv. Mater. 25 (2013) 137–141.
[18] E. Lhuillier, S. Keuleyan, G.-S. Philippe, Optical properties of hgte colloidal quantum dots, Nanotechnology 23 (2012) 175705.
[19] Y. Liu, M. Gibbs, J. Puthussery, S. Gaik, R. Ihly, H. Hillhouse, M. Law, Dependence of carrier mobility on nanocrystal size and ligand length in pbse nanocrystal solids, Nano Lett. 10 (2010) 1960–1969.
[20] C. Kagan, Flexible colloidal nanocrystal electronics, Chem. Soc. Rev. 48 (2018) 1626–1641.
[21] D. Emin, The sign of the Hall effect in hopping conduction, Philos. Mag. A 35 (1977) 1189–1198.
[22] N. Mott, Sign of the Hall effect in Amorphous silicon, Philos. Mag. A B 63 (1991) 3–5.
[23] F. Werner, Hall measurements on low-mobility thin films, J. Appl. Phys. 122 (2017) 135306.
[24] X. Lan, M. Chen, M. Hudson, V. Kamysbayev, Y. Wang, G.-S. Philippe, D. Talapin, Quantum dot solids showing state-resolved band-like transport, Nat. Mater. 19 (2020) 323–329.
[25] J.-S. Lee, M. Kovalenko, J. Huang, D. Chung, D. Talapin, Band-like transport, high electron mobility and high photoconductivity in all-inorganic nanocrystal Arrays, Nat. Nanotechnol. 6 (2011) 348–352.
[26] J.-H. Choi, A. Fafarman, S. Oh, D.-K. Ko, D. Kim, B. Diroll, S. Muramoto, G. Gillen, C. Murray, C. Kagan, Bandlike transport in strongly coupled and doped quantum dot solids: a route to high-performance thin-film electronics, Nano Lett. 12 (2012) 2631–2638.
[27] B. Martinez, C. Livache, N. Goubet, A. Jagtap, H. Cruguel, A. Ouerghi, E. Lacaze, M. Silly, E. Lhuillier, Probing charge carrier dynamics to unveil the role of surface ligands in hgte narrow band gap nanocrystals, J. Phys. Chem. C 122 (2017) 859–865.
[28] M. Kovalenko, M. Scheele, D. Talapin, Colloidal nanocrystals with molecular metal chalcogenide surface ligands, Science 324 (2009) 1417–1420.
[29] J. Jang, D. Dolzhnikov, W. Liu, S. Nam, M. Shim, D. Talapin, Solution-processed transistors using colloidal nanocrystals with composition-matched molecular “solders”: Approaching single crystal mobility, Nano Lett. 15 (2015) 6309–6317.
[30] G. Konstantatos, E. Sargent, Pbs colloidal quantum dot photoconductive photodetectors: transport, traps, and gain, Appl. Phys. Lett. 91 (2007), 173505-173505.
[31] Y. Zhang, D. Hellebusch, N. Bronstein, C. Ko, D. Ogletree, M. Salmeron, A. Alivisatos, Ultrasensitive photodetectors exploiting electrostatic trapping and percolation transport, Nat. Commun. 7 (2016), 11924.
[32] J. Tang, K. Kemp, S. Hoogland, K. Jeong, H. Liu, L. Levina, M. Furukawa, X. Wang, R. Debnath, D. Cha, K.W. Chou, A. Fischer, A. Amassian, J. Asbury, E. Sargent, Colloidal-quantum-dot photovoltaics using atomic-ligand passivation, Nat. Mater. 10 (2011) 765–771.
[33] D.-K. Ko, A. Maurano, S. Suh, D. Kim, G. Hwang, J. Grossman, V. Bulovic, M. Bawendi, Photovoltaic performance of pbs quantum dots treated with metal salts, ACS Nano 10 (2016) 3382–3388.
[34] D. Balazs, D. Dirin, H.-H. Fang, L. Protesescu, G. ten Brink, B.J. Kooi, M. Kovalenko, M. Loi, Counterion-mediated ligand exchange for pbs colloidal quantum dot superlattices, ACS Nano 9 (2015) 11951–11959.
[35] W. Walravens, J. Roo, E. Drijvers, S. ten Brinck, E. Solano, J. Dendooven, C. Detavernier, I. Infante, H. Zeger, Chemically triggered formation of two-dimensional epitaxial quantum dot superlattices, ACS Nano 10 (2016) 6861–6870.
[36] A. Sahu, D. Braga, O. Waser, M.S. Kang, D. Deng, D. Norris, Solid-phase flexibility in Ag2se semiconductor nanocrystals, Nano Lett. 14 (2013) 115–121.
[37] K. Somogyi, G. Sáfrán, Mobility variations in semiconducting Ag2se layers, Vacuum 46 (1995) 1055–1058.
[38] Y. Ding, Y. Qiu, K. Cai, Q. Yao, S. Chen, L. Chen, J. He, High performance N-type Ag2se film on nylon membrane for flexible thermoelectric power generator, Nat. Commun. 10 (2019) 841.
[39] J. Luther, M. Law, Q. Song, C. Perkins, M. Beard, A. Nozik, Structural, optical, and electrical properties of self-Assembled films of pbse nanocrystals treated with 1,2-ethanedithiol, ACS Nano 2 (2008) 271–280.
[40] A. Barkhouse, A. Pattantyus-Abraham, L. Levina, E. Sargent, Thiols passivate recombination centers in colloidal quantum dots leading to enhanced photovoltaic device efficiency, ACS Nano 2 (2008) 2356–2362.
[41] Z. Deng, K. Jeong, G.-S. Philippe, Colloidal quantum dots intraband photodetectors, ACS Nano 8 (2014) 11707–11714.
[42] G. Konstantatos, I. Howard, A. Fischer, S. Hoogland, J. Clifford, E. Klem, L. Levina, E. Sargent, Ultrasensitive solution-cast quantum dot photodetectors, Nature 442 (2006) 180–183.
[43] A.H. Ip, S.M. Thon, S. Hoogland, O. Voznyy, D. Zhitomirsky, R. Debnath, L. Levina, L.R. Rollny, G.H. Carey, A. Fischer, K.W. Kemp, I.J. Kramer, Z. Ning, A.J. Labelle, K.W. Chou, A. Amassian, E.H. Sargent, Hybrid passivated colloidal quantum dot solids, Nat. Nanotechnol. 7 (2012) 577–582.